crystals

MDPI

Article

High-Quality Single-Step Growth of GaAs on C-Plane Sapphire by Molecular Beam

Emmanuel Wangila [1,2,*], Calbi Gunder [1,2], Mohammad Zamani-Alavijeh [1], Fernando Maia de Oliveira [1], Serhii Kryvyi [1], Aida Sheibani [3], Yuriy I. Mazur [1], Shui-Qing Yu [2,4] and Gregory J. Salamo [1,2,3,*]

[1] Institute for Nanoscience and Engineering, University of Arkansas, Fayetteville, AR 72701, USA; cjgunder@uark.edu (C.G.); mzamania@uark.edu (M.Z.-A.); fmaiade@uark.edu (F.M.d.O.); skryvyi@uark.edu (S.K.); ymazur@uark.edu (Y.I.M.)
[2] Material Science and Engineering, University of Arkansas, Fayetteville, AR 72701, USA; syu@uark.edu
[3] Department of Physics, University of Arkansas, Fayetteville, AR 72701, USA; asheiban@uark.edu
[4] Department of Electrical Engineering, University of Arkansas, Fayetteville, AR 72701, USA
* Correspondence: eswangil@uark.edu (E.W.); salamo@uark.edu (G.J.S.)

Abstract: We report on the growth of high-quality GaAs semiconductor materials on an AlAs/sapphire substrate by molecular beam epitaxy. The growth of GaAs on sapphire centers on a new single-step growth technique that produces higher-quality material than a previously reported multi-step growth method. Omega-2theta scans confirmed the GaAs (111) orientation. Samples grown at 700 °C displayed the highest crystal quality with minimal defects and strain, evidenced by narrow FWHM values of the rocking curve. By varying the As/Ga flux ratio and the growth temperature, we significantly improved the quality of the GaAs layer on sapphire, as compared to that obtained in multi-step studies. Photoluminescence measurements at room temperature and 77 K further support these findings. This study underscores the critical role of the As/Ga flux ratio and growth temperature in optimizing GaAs epitaxial growth on sapphire.

Keywords: single-step growth approach; room temperature PL; twinning

Citation: Wangila, E.; Gunder, C.; Zamani-Alavijeh, M.; Maia de Oliveira, F.; Kryvyi, S.; Sheibani, A.; Mazur, Y.I.; Yu, S.-Q.; Salamo, G.J. High-Quality Single-Step Growth of GaAs on C-Plane Sapphire by Molecular Beam. *Crystals* **2024**, *14*, 724. https://doi.org/10.3390/cryst14080724

Academic Editor: Lin Gan

Received: 26 July 2024
Revised: 9 August 2024
Accepted: 11 August 2024
Published: 14 August 2024

1. Introduction

GaAs is a III-V compound semiconductor known for its excellent electronic and optical properties [1,2]. Its direct bandgap makes it highly efficient for light emission and absorption [3], making it ideal for optoelectronic devices like LEDs, laser diodes, and solar cells. GaAs also has high electron mobility, enabling faster electronic devices, which makes it a preferred material for high-frequency and high-speed applications [4], including microwaves.

Combining one of the world's best optical III-V semiconductor materials with one of the best radiofrequency (RF) substrates [5] encourages a potential pathway to achieve the monolithic integration of laser, amplifier, modulator, detector, and microwave devices on a single substrate or fully integrated microwave photonic (IMWP) chip. The sapphire substrate is an attractive IMWP platform due to its low parasitic capacitance, optical transparency, low RF power loss, low cost, and, very uniquely, excellent thermal expansion match to III-V materials for reliability [6–12]. In contrast to silicon, sapphire also provides a low-refractive-index substrate (~1.76) [13,14], allowing the manufacturing of low-loss passive waveguide components. In addition, sapphire has a large bandgap, making it a good candidate for different types of harsh environments [15,16]. On the other hand, the implementation of GaAs on sapphire is complicated by a large lattice mismatch and a different lattice structure between sapphire and GaAs [17], potentially resulting in defects such as twinning, misfit, and threading dislocations, which together can significantly limit material and device performance [18].

In heteroepitaxial systems, strategies like two-step growth, multiple annealing, and strained layer superlattices (SLSs) are employed to manage high lattice mismatch, improve crystal quality, and reduce defects [17]. A previous study combined two-step growth and multiple annealing (multi-step growth) for GaAs epitaxial growth on C-plane sapphire. This study investigated the effects of the growth temperature, V/III ratio, and low-temperature layer growth temperature (LTLGT) on the surface morphology and crystal quality. Optimizing these parameters led to significant improvements, as evidenced by the room-temperature photoluminescence (RT PL) of GaAs on C-plane sapphire [19]. The multi-step approach seemed to us to be a significant improvement over the single-step approach at first. It was quite by accident or even error that we discovered a very unusual and tight window in the As/Ga flux ratio. This resulted in better single-step performance.

Our investigation of the growth of gallium arsenide (GaAs) on sapphire centers on a new single-step growth technique producing higher-quality material than a previously reported multi-step growth method, shown in Figure 1, using AlAs/sapphire as a common substrate [17]. By performing a careful study of (1) the arsenic-to-gallium flux ratio and (2) the growth temperature, we significantly improved the quality of the GaAs layer on sapphire compared to that obtained in multi-step studies [19]. This is evidenced by the observation of monolayer steps that can better meet the stringent requirements for the fabrication of optical laser and detector devices.

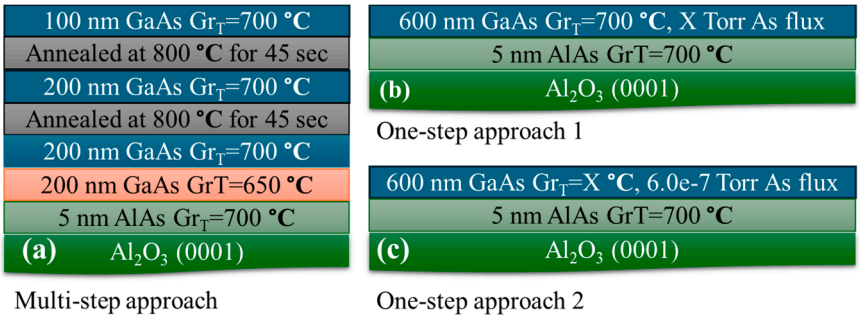

Figure 1. Sample structure for (**a**) previous multi-step GaAs growth approach, (**b**) single-step approach with GaAs grown under varying As flux (x Torr) at constant temperature, and (**c**) single-step growth approach with varying temperature (x °C) at constant As flux.

2. Experimental Design

This study used a Riber-32 molecular beam epitaxy (MBE) ultra-high vacuum (UHV) chamber to grow all samples. Surfacenet GmbH, Rheine, Germany, supplied the sapphire substrates, which were then coated with titanium (Ti) on the backside of each substrate to ensure uniform and efficient heating of the sample during growth. These samples were inserted into a load lock chamber and heated at 200 °C for 1 h to remove water vapor from the substrate. The substrates were moved to a degassing chamber to eliminate organic contaminants and annealed at 900 °C for 6 h. Subsequently, they were transferred into the growth chamber for arsenization by heating the substrate under an arsenic flux of 2×10^{-6} Torr at 650 °C for 30 min to achieve an arsenic-terminated surface.

The As/Ga flux ratio was determined through calibration via an ion gauge built into the manipulator assembly that could be rotated into position to check the BEP. Then, we selected the BEP ratios of As/Ga to use in our investigations. This type of calibration is typical and necessary for all MBE work. The purity of Ga was 7N (99.9999%), while that of As was 7N5 (99.99999%).

The substrate temperature was then adjusted to the growth temperature, and 5 nm of AlAs and 600 nm of GaAs were grown at rates of 0.2 ML/s and 0.8 ML/s, respectively, for all samples (Figure 1). Two approaches were employed for growing GaAs: (1) varying the As/Ga ratios while maintaining a constant temperature of 700 °C, and (2) using an optimized As/Ga ratio while varying the growth temperature. The room-temperature

photoluminescence of these samples was compared with that of the previous sample, S6, which was grown using a multi-step growth method.

The surface morphology during growth was analyzed using reflection high-energy electron diffraction (RHEED) at a glancing angle of 2° with an accelerating voltage of 20 keV and a cathode current of 1.5 A. The RHEED pattern showed a (2 × 2) reconstruction, indicating that the GaAs surface is a Ga-terminated GaAs (111)A surface [8]. The surface morphology was studied ex situ using an atomic force microscopy (AFM, Bruker Dimension 3000) device manufactured in the USA (Billerica, Billerica, MA, USA). This was performed with a silicon (Si) tip with a radius of 10 nm, optimized for feedback and force parameters to ensure stable performance. The crystal quality and epitaxial orientation were determined using X-ray diffraction (XRD). This system consisted of a Paralytical X′Pert MRD diffractometer utilizing a CuKα1 source (λ = 0.15406) from Almelo, located in the Netherlands. Photoluminescence (PL) measurements were conducted in a closed-cycle helium cryostat utilizing a frequency-doubled neodymium-doped yttrium aluminum garnet laser manufactured in France (Lille), with a spot size between 1 and 2 μm and optical power of about 5 mW. InGaAs photodiode detector arrays cooled with liquid nitrogen were used to detect PL signals dispersed by a monochromator. Both the detector and monochromator were also made in France (Lille).

3. Results and Discussion

GaAs growth on C-plane sapphire involves managing the significant lattice mismatch between sapphire's hexagonal crystal structure and the cubic zinc-blend structure of GaAs. In previous work on the multi-step growth of GaAs on sapphire [19], it was found that the growth of a thin initial AlAs layer (5 nm) on sapphire before the addition of GaAs wet the surface more uniformly when compared to the growth of GaAs directly on sapphire. The use of the wetting layer was continued for our investigation of a single-step growth approach. For this study, the AlAs/sapphire was taken as our starting substrate for all samples. To investigate the single-step approach, we examined the effects of the As flux and growth temperature on the crystalline quality. The approach was divided into two distinct methods. In method (a), the As/Ga flux ratio was varied while a constant growth temperature was maintained. This approach allowed us to analyze how different As/Ga ratios affected the RHEED pattern, crystal morphology, and photoluminescence (PL) properties of GaAs samples. In method (b), the optimized As/Ga ratio was selected from section (a) to remain constant, and then we investigated the effect of different substrate growth temperatures on the RHEED, PL, and surface morphology. By examining the results from both methods, we aimed to improve the surface smoothness by identifying the optimal growth conditions for producing high-quality GaAs epitaxial layers on a sapphire platform. The observations and discussion of the results from each method are presented below.

(a) Growth of GaAs at Different Values of As/Ga Flux Ratio at Constant Growth Temperature

In this study, we explored the impact of varying the As/Ga flux ratio on three GaAs thin films (samples S1, S2, and S3) grown on C-plane sapphire substrates, all at a growth temperature of 700 °C. The experiment started with an As beam equivalent pressure (BEP) of 3.6×10^{-6} Torr, corresponding to an As/Ga flux ratio of 15:1. To find the optimal flux ratio, we systematically increased the arsenic flux. The final flux ratios for samples S1, S2, and S3 were 15:1, 25:1, and 30:1, respectively. These ratios represent the extreme range on both sides of the optimal value.

The surface morphology of the samples was examined using AFM, displaying well-arranged triangular-shaped features, as shown in Figure 2. The analysis indicated surface roughness values of 37.8 nm for S1, 3.58 nm for S2, and 6.36 nm for S3. These results indicate that the two samples grown with the higher As/Ga flux ratios were more favorable for the growth of GaAs at 700 °C.

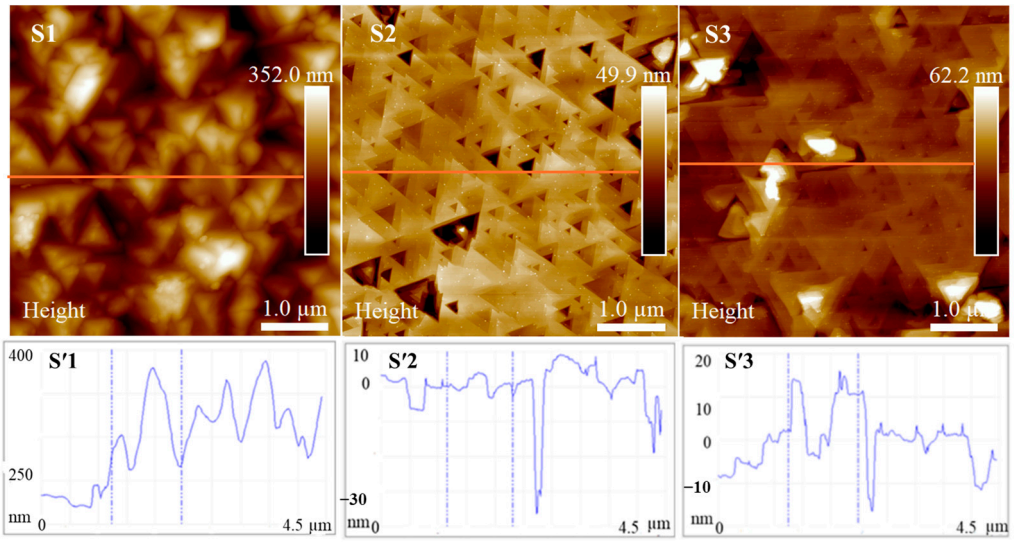

Figure 2. AFM images of samples **S1** (BEP ratio of 15:1), **S2** (BEP ratio of 25:1), and **S3** (BEP ratio of 30:1) with horizontal line scans for each sample labeled **S′1**, **S′2** and **S′3** respectively.

Under in situ characterization, the RHEED images of samples S2 and S3 displayed streaky patterns, while sample S1 exhibited a spotty pattern interspersed with streaks (see Figure 3). The streaky patterns observed in samples S2 and S3 indicate smooth, well-ordered surfaces with a uniform atomic arrangement, suggesting a high degree of crystalline order and layer-by-layer (2D) growth. In contrast, the RHEED pattern of sample S1, which showed both spotty and streaky features, indicates the presence of 3D islands or clusters. This suggests a transition from 2D to 3D growth modes. These observations agree with the surface roughness shown by AFM.

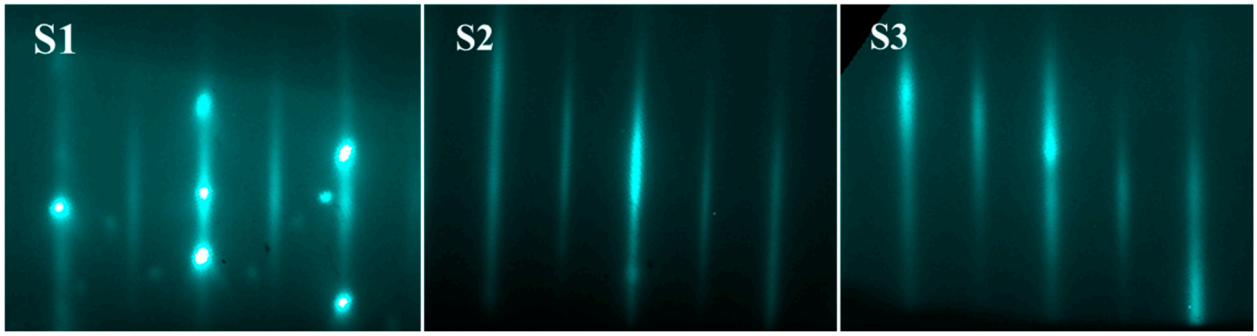

Figure 3. The RHEED image of sample S1 displays a streaky pattern interspersed with a spotty pattern, while samples S2 and S3 show only a streaky pattern.

The crystallographic quality of the films was investigated using XRD omega rocking curve scans. As presented in Figure 4, the rocking curves were fitted with Pseudo-Voigt functions. The full width at half-maximum (FWHM) values of the peaks for GaAs samples S1, S2, and S3 are presented in Table 1.

Overall, sample S2 with an As/Ga ratio of 25:1 exhibited the smallest FWHM, indicating its higher crystal quality. The broadest FWHM was seen for sample S1, and this is likely due to insufficient As flux relative to Ga causing a higher defect density and poorer crystal quality than those in samples S2 and S3. This supports Erickson et al.'s [20] finding that low As pressure results in rougher films and higher defect density, emphasizing the importance of adequate arsenic flux for better film quality. These findings are consistent with the AFM results, which provide insight into the surface morphology and roughness of the samples. The smoother surface of sample S2 corresponds to the narrow FWHM values, reflecting better crystal quality with fewer defects and lower strain. The higher surface

roughness observed in sample S3 correlates with the broad FWHM values, suggesting a higher degree of surface imperfections, strain, and defects within the crystal structure.

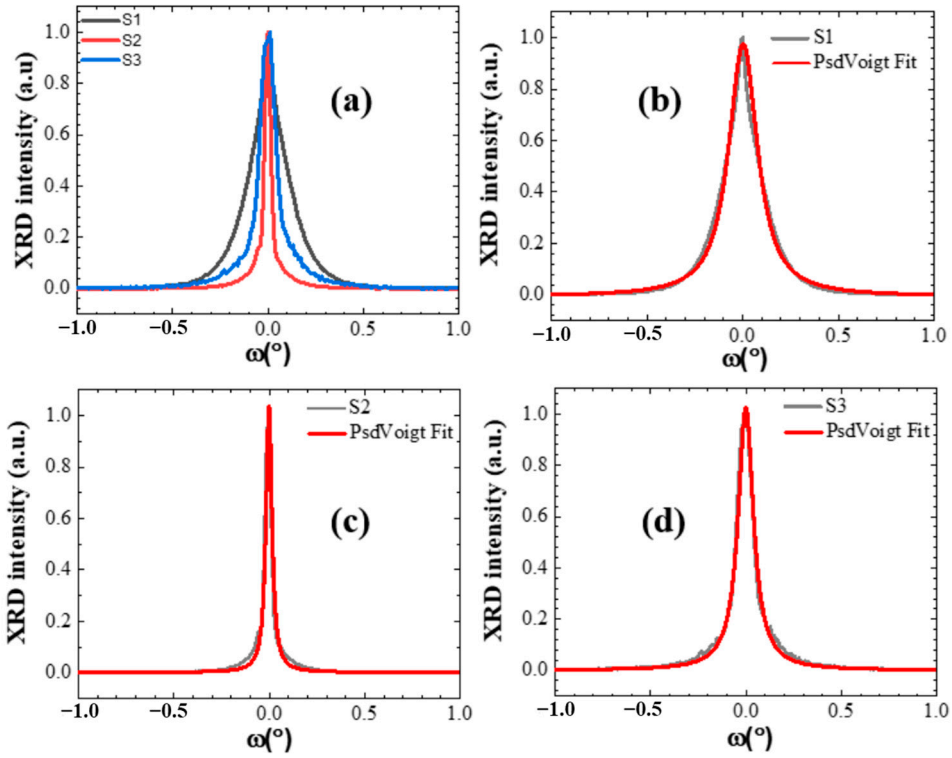

Figure 4. (**a**) Normalized XRD omega rocking curve scans of samples S1, S2, and S3. (**b**–**d**) Pseudo-Voigt fitting of the rocking curves to determine the FWHM of the samples.

Table 1. FWHM values of XRD omega rocking curve scans for the Pseudo-Voigt components, As/Ga flux ratios, and surface roughness values for samples S1, S2, and S3 (all samples were grown at 700 °C).

Sample Name	FWHM (deg)	As/Ga Flux Ratio	Surface Roughness (nm)
S1	0.2040	15:1	37.8
S2	0.0373	25:1	3.58
S3	0.097	30:1	6.36

The orientation of the GaAs films was determined using the XRD omega-2theta (ω-2θ) scans. In our study, the ω-2θ scans revealed that GaAs films predominantly grew in the (111) orientation. This was indicated by the presence of a strong diffraction peak corresponding to the (111) planes of GaAs, as shown in Figure 5a, suggesting that these planes are parallel to the substrate surface and represent the preferred orientation during growth. An AFM analysis further confirmed this preferred GaAs (111) orientation by evidencing well-arranged triangular-shaped facets on the surface, which are characteristic of the (111) orientation, as observed by Emmanuel et al. in the growth of Ge on sapphire [21] and by Schuck et al. in the growth of GaAs quantum dots [22].

The crystallographic orientation and symmetry of the crystals were further determined using XRD phi (φ) scans, in which a sample is rotated around an axis perpendicular to its surface. This allows for the measurement of diffraction peaks that reveal crystal plane symmetry and alignment [23]. This technique is particularly useful for identifying misalignment or secondary crystallographic orientations within the sample. In our study, φ scanning was conducted on the (220) planes of GaAs to examine the in-plane symmetry of the grown films. Ideally, GaAs (111) should exhibit three peaks, reflecting the threefold

symmetry of GaAs (111) [24]. However, in our samples, we observed not only three dominant peaks corresponding to the primary orientation but also three minor peaks representing another domain (see Figure 5b). This domain represents the twin of the primary orientation, as observed on zinc blende InAs (111) [25]. The presence of minor peaks alongside the dominant peaks suggests the existence of twin domains, which are secondary crystallographic orientations where portions of the crystal are mirror images of the main orientation. These twin domains, or twins, indicate a degree of misalignment and structural imperfections at the twin boundaries within the GaAs films. The ratio between the intensities of the low- and high-intensity peaks was measured for each sample, yielding 16.8 ± 0.1% for sample S1, 11.6 ± 0.5% for sample S2, and 17.9 ± 0.5% for sample S3.

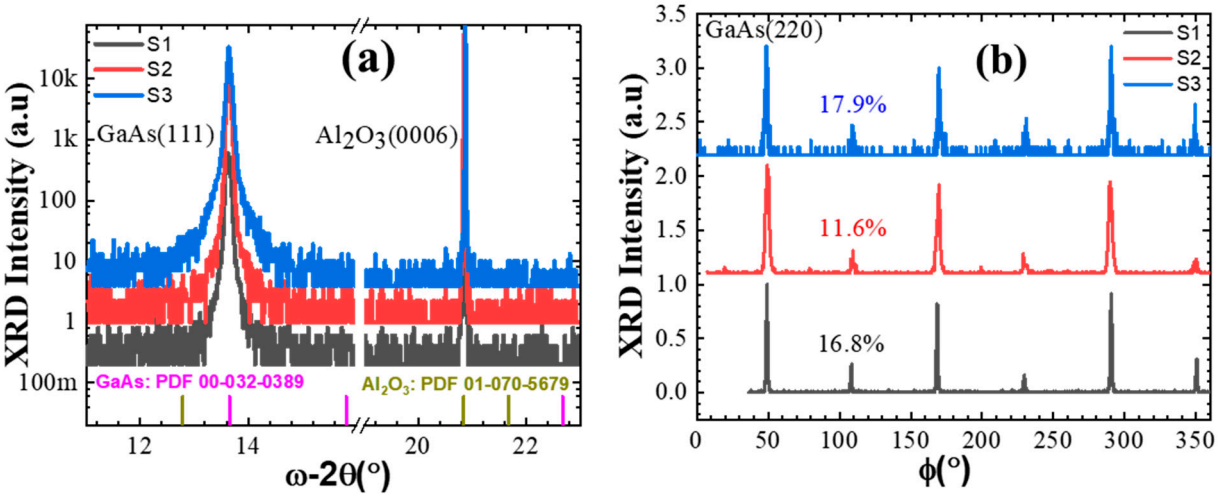

Figure 5. XRD results of samples S1, S2, and S3: (**a**) omega-2theta scan with corresponding ICDD database references and (**b**) phi scan.

The lowest ratio of 11.6% seen for sample S2 indicates its highest degree of preferred orientation (111) with minimal twinning. This correlates well with the earlier observations from the ω-2θ scan and AFM analysis, which showed sample S2 having the highest crystal quality and the smoothest surface morphology. Samples S1 and S3, with ratios of 16.8% and 17.9% respectively, exhibit more pronounced twinning than sample S1. This is consistent with the broad FWHM values observed in the diffraction peaks and the moderate surface roughness measured by AFM, indicating a higher degree of defects and strain.

The optical properties of the GaAs layers were investigated by PL, as shown in Figure 6. At room temperature (RT), the PL emission of sample S2 was observed at 1.431 eV, with higher intensity, followed by sample S3 at 1.428 eV and sample S1 at 1.426 eV with the lowest intensity. The high PL intensity of sample S2 indicates more efficient radiative recombination, suggesting better crystal quality and fewer defects [26]. Moreover, the shift in PL emission towards lower energies for samples S1 and S3 can be attributed to strain and defects altering the band structure. These defects introduce states within the bandgap, leading to pathways of non-radiative recombination. At 77 K, the low-temperature (LT) PL measurements displayed emission at 1.501 eV for sample S1, 1.508 eV for sample S2, and 1.503 eV for sample S3. The overall higher intensity of PL emission at LT is due to reduced thermal vibrations and enhanced exciton binding, leading to more efficient radiative recombination [26,27]. Additionally, the closer proximity of atoms at LT increases the binding energy between them, shifting the bandgap towards higher energies (Figure 6b). Thermal vibrations, which are more pronounced at higher temperatures, reduce the carrier lifetime in excited states, broadening the PL linewidth, as evidenced by the wider spectral linewidth of the RT PL of all samples (Figure 6a). Based on the PL results, sample S2 exhibited a better overlap between electron and hole wavefunctions [28]. This results in more efficient radiative recombination and intense light emission. In contrast, the low PL

intensity of sample S1 indicates higher strain and defect density, which is consistent with its lower As flux and higher Ga-related defect formation [20].

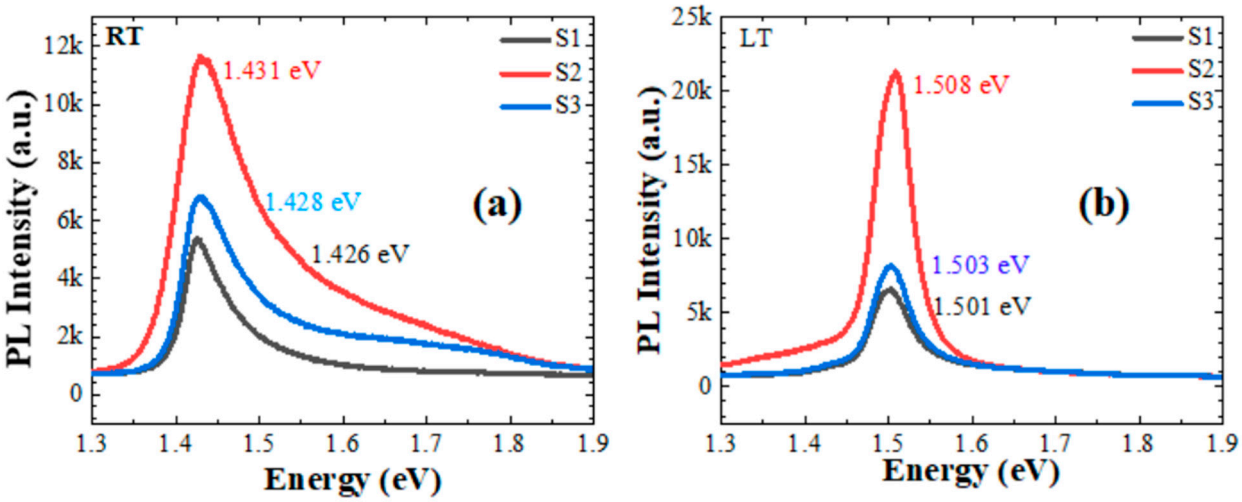

Figure 6. PL emission of samples S1, S2, and S3 at (**a**) room temperature (RT) and (**b**) low temperature (LT) at 77 K.

(b) Growth of GaAs at Different Growth Temperatures at Constant As/Ga Flux Ratio

Based on the results of section (a), sample S2 grown using the 25:1 ratio exhibited the best crystal quality and most intense radiative emission. Hence, to further study the effect of growth parameters on the quality of GaAs, two additional samples were grown at temperatures of 720 °C (sample S4) and 690 °C (sample S5).

By analyzing the crystal quality of GaAs grown at different temperatures, we can observe how desorption affects epitaxial growth. High temperatures during epitaxy can trigger As atom desorption from the surface, which reduces the effective As flux at the growth surface, even with constant As flux [29]. Consequently, an imbalanced As/Ga ratio may occur, favoring the formation of gallium-rich GaAs layers, which exhibit distinct electronic properties and crystal structures as compared to stoichiometric GaAs [30]. The temperature also influences atom mobility during growth. Higher temperatures, such as 720 °C for S5, increase atom mobility, which can lead to either a smoother or rougher surface depending on the balance between adatom diffusion and desorption rates. In contrast, slightly lower temperatures, such as 690 °C for S4, may reduce atom mobility, potentially leading to less optimal surface quality. Sample S2, grown at 700 °C, represents an intermediate temperature that balances atom mobility to achieve desirable surface and optical properties.

The XRD omega rocking curve scans shown in Figure 7 illustrate the contrast between the growth processes at different temperatures. Sample S4, grown at a lower temperature of 690 °C, exhibited an FWHM of the GaAs film bulk of 0.03967 degrees, which indicates relatively good crystal quality, suggesting minimal defect propagation. Conversely, Sample S5, grown at a higher growth temperature of 720 °C, had a larger FWHM value of 0.11339 degrees, suggesting lower crystal quality with more defects.

The XRD φ scan results shown in Figure 8b reveal the degree of twinning in the GaAs samples grown at different temperatures. Sample S2, grown at 700 °C, had a twinning area ratio of 11.6%, indicating minimal secondary crystallographic orientations and a well-aligned crystal structure. In contrast, Sample S4, grown at 690 °C, exhibited a high twinning ratio of 38.3%, suggesting significant secondary orientations or misalignment within the crystal structure at this lower temperature. Despite the high twinning ratio, the XRD ω scan results for S4 demonstrated relatively good crystal quality (see Figure 7a). Sample S5, grown at 720 °C, showed a twinning ratio of 11.6%, similar to that for S2, indicating minimal twinning. The XRD φ scan data are summarized in Table 2. Additionally, the

GaAs (111) orientation as observed in the Omega-2Theta scan (Figure 8a) further confirms the crystallographic quality of the samples. However, sample S5 exhibited the lowest XRD intensity, which can be attributed to desorption effects at the higher growth temperature, reducing the crystallographic quality when compared to samples S1 and S4.

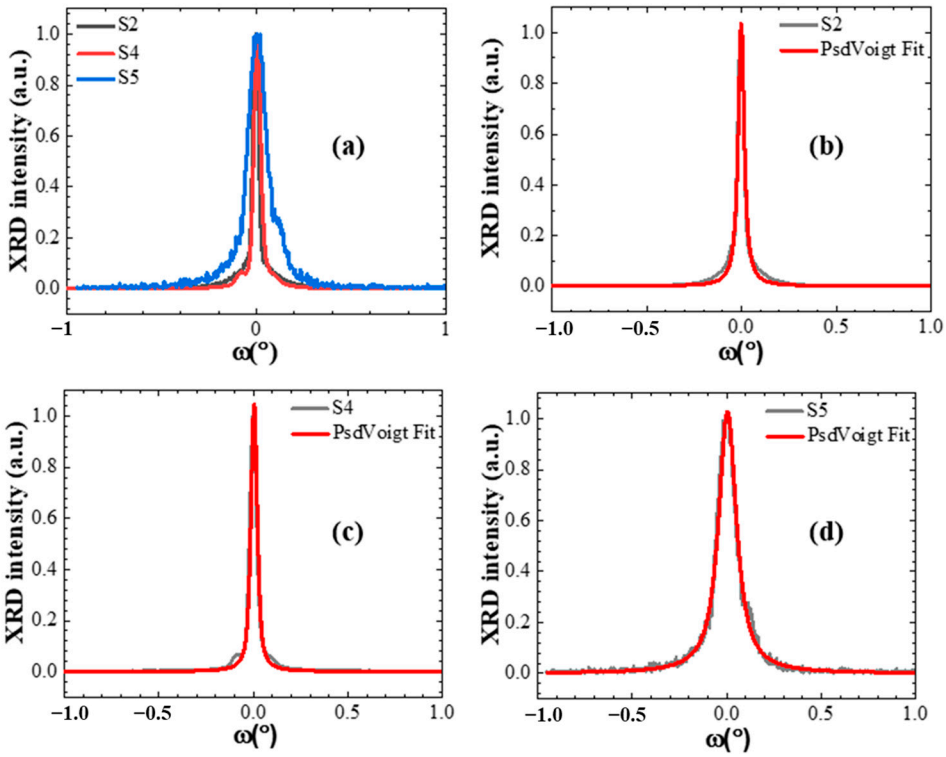

Figure 7. (**a**) XRD omega rocking curve scans for samples S2, S4, and S5. (**b**–**d**) Pseudo-Voigt fittings for each sample.

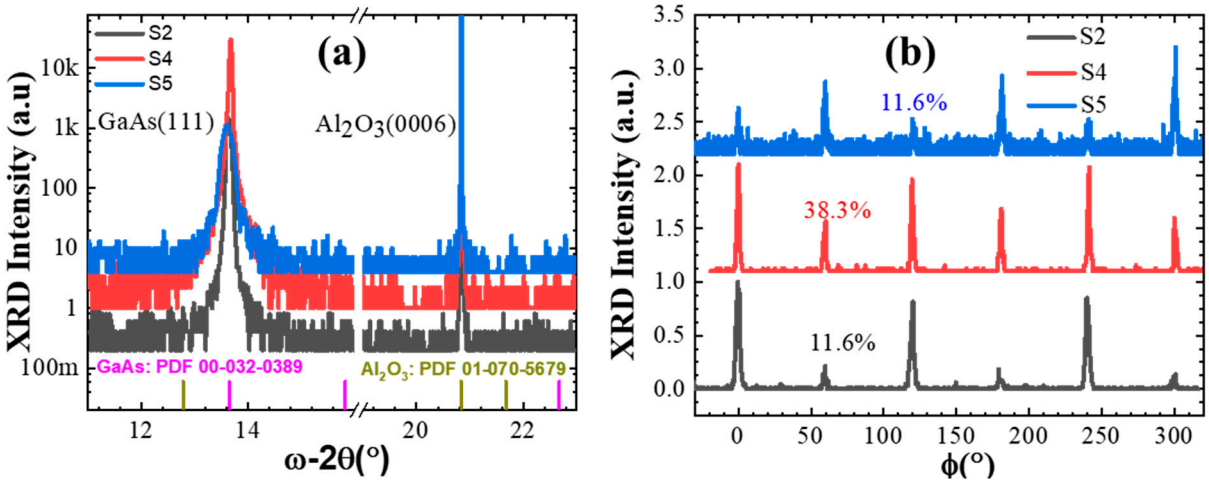

Figure 8. XRD results of samples S2, S4, and S5: (**a**) omega-2theta scan with corresponding ICDD database references and (**b**) phi scan.

The AFM analysis of samples S2 and S4 further supports these observations (Figure 9). Both samples showed triangular-shaped features, indicating well-ordered (111) facets. However, sample S4's triangular features mostly faced the opposite direction compared to those in sample S2, which supports the high ratio of twinning observed in the XRD φ scan. These features are consistent with high-quality crystal growth, as observed in the XRD ω scan results. However, sample S5 showed coalescence on the surface, obscuring the

triangular features and high surface roughness. This degradation in surface morphology at higher temperatures is likely due to increased As desorption, resulting in a Ga-rich surface and higher defect density. The surface roughness of sample S2 was 3.58 nm, that of sample S4 was 18.3 nm, and that of sample S5 was 8.71 nm. The temperature and As flux play crucial roles in determining surface features. At optimal temperatures, such as 700 °C for sample S2, sufficient As is incorporated into the growing film, leading to well-ordered (111) facets and minimal defects. At slightly lower temperatures, such as 690 °C for sample S4, the crystal quality remains high, although structural imperfections may arise. At higher temperatures, such as 720 °C for sample S5, increased desorption rates reduce the effective As flux, leading to an imbalanced As/Ga ratio. This results in Ga-rich GaAs layers with higher defect density, coalescing surface features, and increased surface roughness.

Table 2. Twinning ratio, surface roughness, and FWHM of XRD omega rocking curve scans for samples S2, S4, and S5 (all samples grown at constant As/Ga flux ratio of 25:1).

Sample Name	Twinning Ratio (%)	Surface Roughness (nm)	FWHM (deg)
S2	11.6	3.58	0.03725
S4	38.3	18.3	0.03967
S5	11.6	8.71	0.11339

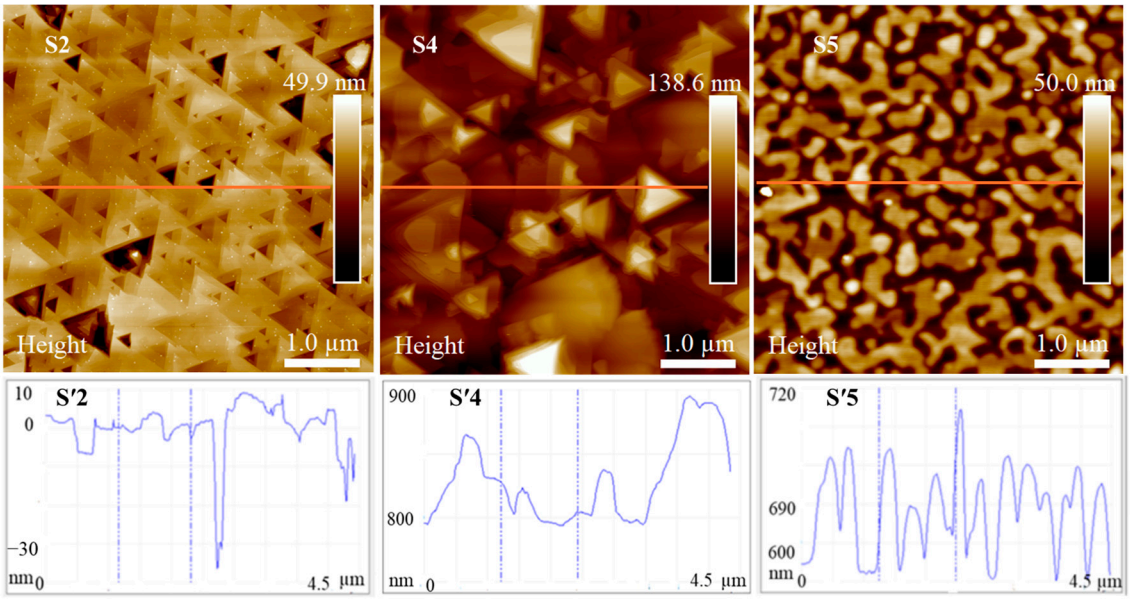

Figure 9. AFM images of samples (**S2**) grown at 700 °C, (**S4**) 690 °C, and (**S5**) 720 °C with horizontal line scan for each sample labelled **S′2**, **S′4**, **S′5** respectively (samples grown with a BEP ratio of 25:1).

The XRD ω-2θ analysis still indicated that the GaAs samples predominantly exhibited a (111) orientation, which aligns with the findings from the XRD ω scan and AFM analysis. This technique allows for the measurement of diffraction peaks corresponding to specific crystallographic planes, providing a detailed understanding of the preferred orientation of the crystal. In our study, the XRD ω-2θ scan confirmed the (111) orientation of GaAs for all samples. Despite the variations in crystal quality observed in the XRD ω scan and AFM results, the GaAs films consistently showed a strong diffraction peak corresponding to the (111) planes. This suggests that, regardless of the temperature variations and resulting defects or surface coalescence, the primary crystallographic orientation remained (111).

The optical properties of the samples grown at different temperatures were investigated by PL, as shown in Figure 10. The RT and LT PL measurements revealed significant information about the optical properties and crystal quality of the GaAs samples. At 77 K, both samples S1 and S4 displayed a clear PL emission at 1.509 eV, suggesting reduced

thermal vibrations and improved exciton binding [26,31]. This indicates high optical quality and fewer defects at low temperatures, with similar excitonic behavior and band structure properties for both samples. Notably, sample S4 also exhibited a minor PL emission around 1.42 eV at LT, which indicates the presence of additional defect states or impurities within the crystal structure creating localized energy levels affected by crystal quality. The absence of a detectable PL emission in sample S5 at both RT and LT further confirms its poor crystal quality, with significant non-radiative recombination pathways preventing PL emission [30].

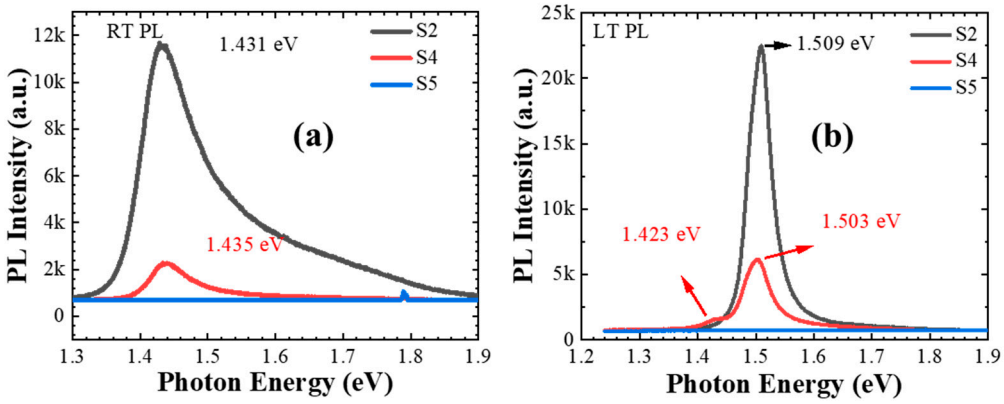

Figure 10. PL emission of samples S2, S4, and S5 at (**a**) room temperature (RT) and (**b**) low temperature (LT) at 77 K.

The PL data are consistent with the structural analysis results from XRD ω scans and AFM. Sample S2 exhibited high crystal quality with minimal defects, indicated by narrow FWHM values in the XRD ω scan and well-ordered triangular features observed via AFM. Sample S4, despite having a higher twin ratio, maintained relatively good crystal quality, evidenced by the presence of RT PL emission energy and strong PL intensity at 77 K, indicating minimal strain and defect density. Its PL intensity was quite high for both room and low temperatures, in contrast to that for sample S5.

Comparing single-step to multi-step growth revealed that the single-step approach for GaAs growth simplifies the process and achieves the desired optical properties without the need for annealing. Figure 11a shows the RT PL emissions of sample S6 and the reference sample of GaAs (111), while Figure 11b,c display the RT PL emissions of the samples grown using the single-step approach. Moreover, the single-step method resulted in a significantly smoother surface [7], which is key to the fabrication of advanced photonic and electronic devices. This indicates the advantage of single-step growth over multi-step growth.

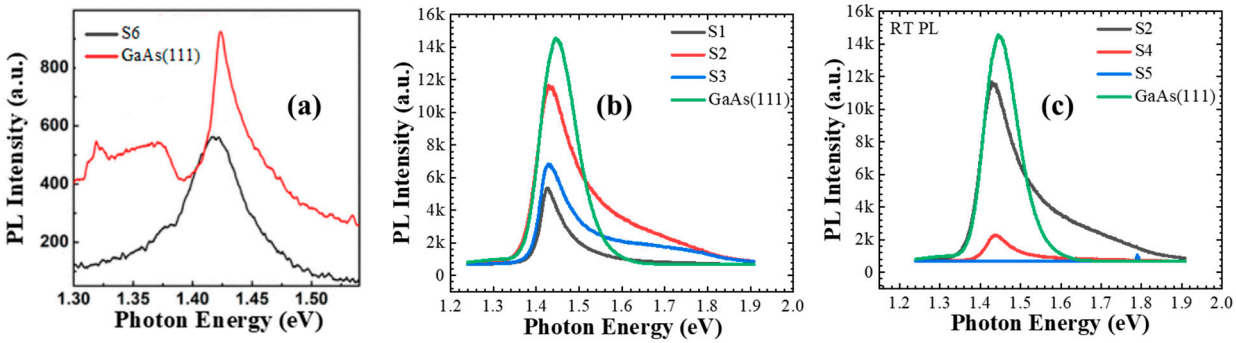

Figure 11. RT PL for GaAs from (**a**) previous publication using multi-step approach [7], (**b**) single-step approach 1 for samples S1, S2, and S3 grown at 700 °C with different BEP ratios of 15:1, 25:1, and 30:1 respectively, and (**c**) single-step approach 2 for samples S1, S4, and S5 (grown at different temperatures with same BEP ratio of 25:1).

4. Conclusions

This research demonstrated that the single-step growth process for gallium arsenide (GaAs) on an aluminum arsenide (AlAs) sapphire substrate produces GaAs films with significantly higher crystal and optical quality in comparison to the previous reports on the multi-step method. The multi-step method requires an annealing phase, involving additional heating and cooling cycles, increasing the overall processing time. This single-step approach, on the other hand, eliminates multiple steps and intermediate annealing, allowing continuous epitaxial growth. By optimizing the growth temperature and maintaining a high arsenic-to-gallium flux ratio, the single-step process achieves a smoother surface finish, as well as narrower rocking curve FWHM values and photoluminescence linewidths. By careful study of (1) the arsenic-to-gallium flux ratio and (2) the growth temperature, we achieved the growth of an improved two-dimensional GaAs surface, potentially ready for advanced photonic and electronic devices.

Author Contributions: Conceptualization, E.W., S.-Q.Y. and G.J.S.; methodology, E.W. and C.G.; software, E.W. and C.G.; validation, E.W., C.G. and G.J.S.; formal analysis, E.W., F.M.d.O., S.K. and Y.I.M.; investigation, E.W., C.G., M.Z.-A. and A.S.; resources, E.W., M.Z.-A. and C.G.; data curation, E.W., F.M.d.O., S.K. and C.G.; writing—original draft preparation, E.W.; writing—review and editing, E.W., C.G., S.K., F.M.d.O., A.S., M.Z.-A., Y.I.M., S.-Q.Y. and G.J.S.; visualization, E.W. and C.G.; supervision, S.-Q.Y. and G.J.S.; project administration, S.-Q.Y. and G.J.S.; funding acquisition, S.-Q.Y. and G.J.S. All authors have read and agreed to the published version of the manuscript.

Funding: This project was funded by Navy, entitled "SiGeSnPb Semiconductor Fab for Room Temp Electro-Optic Infrared (IR) Sensors". Sponsor Award ID: N00014-23-1-2008. It was also funded by MURI, entitled "Understanding and Breaking the Material Barriers of SiGeSn Alloys for Infrared Devices". Sponsor Award ID: FA9550-19-1-0341.

Data Availability Statement: The original contributions presented in the study are included in the article; further inquiries can be directed to the corresponding author.

Acknowledgments: We would like to acknowledge the tireless efforts of Emily in contacting the company that supplies liquid nitrogen to MBE lab.

Conflicts of Interest: The authors declare no conflicts of interest.

References

1. Balaghi, L.; Shan, S.; Fotev, I.; Moebus, F.; Rana, R.; Venanzi, T.; Hübner, R.; Mikolajick, T.; Schneider, H.; Helm, M.; et al. High electron mobility in strained GaAs nanowires. *Nat. Commun.* **2021**, *12*, 6642. [CrossRef]
2. Chu, M.; Sun, Y.; Aghoram, U.; Thompson, S.E. Strain: A solution for higher carrier mobility in nanoscale MOSFETs. *Annu. Rev. Mater. Res.* **2009**, *39*, 203–229. [CrossRef]
3. Huang, J.; Yang, W.; Chen, Z.; Yang, S.; Xue, K.H.; Miao, X. Why Is the Bandgap of GaP Indirect While That of GaAs and GaN Are Direct? *Phys. Status Solidi (RRL)–Rapid Res. Lett.* **2024**, *18*, 2300489. [CrossRef]
4. Joyce, H.J.; A Baig, S.; Parkinson, P.; Davies, C.L.; Boland, J.L.; Tan, H.H.; Jagadish, C.; Herz, L.M.; Johnston, M.B. The influence of surfaces on the transient terahertz conductivity and electron mobility of GaAs nanowires. *J. Phys. D Appl. Phys.* **2017**, *50*, 224001. [CrossRef]
5. Azhan, N.H.; Su, K.; Okimura, K.; Sakai, J. Radio frequency substrate biasing effects on the insulator-metal transition behavior of reactively sputtered VO2 films on sapphire (001). *J. Appl. Phys.* **2015**, *117*, 185307. [CrossRef]
6. Katyba, G.M.; Zaytsev, K.I.; Dolganova, I.N.; Shikunova, I.A.; Chernomyrdin, N.V.; Yurchenko, S.O.; Komandin, G.A.; Reshetov, I.V.; Nesvizhevsky, V.V.; Kurlov, V.N. Sapphire shaped crystals for waveguiding, sensing and exposure applications. *Prog. Cryst. Growth Charact. Mater.* **2015**, *64*, 133–151. [CrossRef]
7. Wang, Z.; Sun, K.; Xie, P.; Liu, Y.; Gu, Q.; Fan, R.; Wang, J. Epsilon-negative BaTiO3/Cu composites with high thermal conductivity and yet low electrical conductivity. *J. Mater.* **2020**, *6*, 145–151. [CrossRef]
8. Aggarwal, R.L.; Ramdas, A.K. *Physical Properties of Diamond and Sapphire*; CRC Press: Boca Raton, FL, USA, 2019.
9. Sp, T.S.; Nguyen, P.T.T.; Do, N.H.N.; Le, D.K.; Thai, Q.B.; Le, P.K.; Phan-Thien, N.; Duong, H.M. Advanced fabrication and multi-properties of aluminium hydroxide aerogels from aluminium wastes. *J. Mater. Cycles Waste Manag.* **2021**, *23*, 885–894. [CrossRef]
10. Liang, J.; Nakamura, Y.; Zhan, T.; Ohno, Y.; Shimizu, Y.; Katayama, K.; Watanabe, T.; Yoshida, H.; Nagai, Y.; Wang, H.; et al. Fabrication of high-quality GaAs/diamond heterointerface for thermal management applications. *Diam. Relat. Mater.* **2021**, *111*, 108207. [CrossRef]

11. Zhou, S.; Zhao, X.; Du, P.; Zhang, Z.; Liu, X.; Liu, S.; Guo, L.J. Application of patterned sapphire substrate for III-nitride light-emitting diodes. *Nanoscale* **2022**, *14*, 4887–4907. [CrossRef]
12. Katyba, G.M.; Zaytsev, K.I.; Chernomyrdin, N.V.; Shikunova, I.A.; Komandin, G.A.; Anzin, V.B.; Lebedev, S.P.; Spektor, I.E.; Karasik, V.E.; Yurchenko, S.O.; et al. Sapphire photonic crystal waveguides for terahertz sensing in aggressive environments. *Adv. Opt. Mater.* **2018**, *6*, 1800573. [CrossRef]
13. Chomsaeng, N.; Sukcharoen, S.; Meechoowas, E. Lithium-Cobalt Glass for Sapphire. *Key Eng. Mater.* **2016**, *702*, 108–112. [CrossRef]
14. Ko, Y.H.; Yu, J.S. Highly transparent sapphire micro-grating structures with large diffuse light scattering. *Opt. Express* **2011**, *19*, 15574–15583. [CrossRef] [PubMed]
15. Yang, D.; Kim, B.; Eom, T.H.; Park, Y.; Jang, H.W. Epitaxial growth of alpha gallium oxide thin films on sapphire substrates for electronic and optoelectronic devices: Progress and perspective. *Electron. Mater. Lett.* **2022**, *18*, 113–128. [CrossRef]
16. Tsao, J.Y.; Chowdhury, S.; Hollis, M.A.; Jena, D.; Johnson, N.M.; Jones, K.A.; Kaplar, R.J.; Rajan, S.; Van de Walle, C.G.; Bellotti, E.; et al. Ultrawide-bandgap semiconductors: Research opportunities and challenges. *Adv. Electron. Mater.* **2018**, *4*, 1600501. [CrossRef]
17. Kumar, R.; Saha, S.K.; Kuchuk, A.; Maidaniuk, Y.; de Oliveira, F.M.; Yan, Q.; Benamara, M.; Mazur, Y.I.; Yu, S.-Q.; Salamo, G.J. GaAs layer on c-plane sapphire for light emitting sources. *Appl. Surf. Sci.* **2021**, *542*, 148554. [CrossRef]
18. Simoen, E. Impact of defects on the performance of high-mobility semiconductor devices. In *High Mobility Materials for CMOS Applications*; Woodhead Publishing: Cambridge, UK, 2018; pp. 159–203.
19. Kumar, R.; Saha, S.K.; Kuchuk, A.; Maia de Oliveira, F.; Khiangte, K.R.; Yu, S.Q.; Mazur, Y.I.; Salamo, G.J. Improving the Material Quality of GaAs Grown on the c-Plane Sapphire by Molecular Beam Epitaxy to Achieve Room-Temperature Photoluminescence. *Cryst. Growth Des.* **2023**, *23*, 7385–7393. [CrossRef]
20. Erickson, L.P.; Mattord, T.J.; Carpenter, G.L.; Palmberg, P.W.; Pearah, P.J.; Klein, M.V.; Morkoç, H. Effect of substrate temperature on molecular beam epitaxial GaAs growth using As2. *J. Appl. Phys.* **1984**, *56*, 2231–2235. [CrossRef]
21. Wangila, E.; Gunder, C.; Lytvyn, P.M.; Zamani-Alavijeh, M.; de Oliveira, F.M.; Kryvyi, S.; Stanchu, H.; Sheibani, A.; Mazur, Y.I.; Yu, S.-Q.; et al. The Epitaxial Growth of Ge and GeSn Semiconductor Thin Films on C-Plane Sapphire. *Crystals* **2024**, *14*, 414. [CrossRef]
22. Schuck, C.F.; Vallejo, K.D.; Garrett, T.; Yuan, Q.; Wang, Y.; Liang, B.; Simmonds, P.J. Impact of arsenic species on self-assembly of triangular and hexagonal tensile-strained GaAs (111) A quantum dots. *Semicond. Sci. Technol.* **2020**, *35*, 105001. [CrossRef]
23. Martinez-Tomas, M.C.; Montenegro, D.N.; Sallet, V.; Munoz-Sanjosé, V. High resolution x-ray diffraction methodology for the structural analysis of one-dimensional nanostructures. *J. Appl. Phys.* **2012**, *112*, 014305. [CrossRef]
24. Lu, Z.; Wen, X.; Washington, M.A.; Lu, T.M. Heteroepitaxy of High-Mobility Germanium on Sapphire (0001) with Magnetron Sputtering. *ACS Appl. Electron. Mater.* **2020**, *2*, 1635–1644. [CrossRef]
25. Pal, S.; Singh, S.; Dixit, V.; Sharma, T.; Kumar, R.; Sinha, A.; Sathe, V.; Phase, D.; Mukherjee, C.; Ingale, A. Crystalline and band alignment properties of InAs/Ge (111) heterostructure. *J. Alloys Compd.* **2015**, *646*, 393–398. [CrossRef]
26. Huang, J.-Y.; Shang, L.; Ma, S.-F.; Han, B.; Wei, G.-D.; Liu, Q.-M.; Hao, X.-D.; Shan, H.-S.; Xu, B.-S. Low temperature photoluminescence study of GaAs defect states. *Chin. Phys. B* **2020**, *29*, 010703. [CrossRef]
27. Harris, T.R. Optical Properties of Si, Ge, GaAs, GaSb, InAs, and InP at Elevated Temperatures. Master's Thesis, Air University, Islamabad, Pakistan, 2010.
28. del Águila, A.G.; Groeneveld, E.; Maan, J.C.; Donegá, C.d.M.; Christianen, P.C.M. Effect of electron-hole overlap and exchange interaction on exciton radiative lifetimes of CdTe/CdSe heteronanocrystals. *ACS Nano* **2016**, *10*, 4102–4110. [CrossRef] [PubMed]
29. Berrie, C.L.; Leone, S.R. Desorption of arsenic species during the surfactant enhanced growth of Ge on Si (100). *J. Phys. Chem. B* **2002**, *106*, 6488–6493. [CrossRef]
30. LaBella, V.P.; Krause, M.R.; Ding, Z.; Thibado, P.M. Arsenic-rich GaAs (0 0 1) surface structure. *Surf. Sci. Rep.* **2005**, *60*, 1–53. [CrossRef]
31. Vulic, N.; Goodnick, S.M. Analysis of recombination processes in polytype gallium arsenide nanowires. *Nano Energy* **2019**, *56*, 196–206. [CrossRef]